ACS NANO

www.acsnano.org

ARTICLE

Self-Locomotive Soft Actuator Based on Asymmetric Microstructural $Ti_3C_2T_x$ MXene Film Driven by Natural Sunlight Fluctuation

Ying Hu,* Lulu Yang, Qiuyang Yan, Qixiao Ji, Longfei Chang, Chenchu Zhang, Jian Yan, Ranran Wang,* Lei Zhang, Guan Wu,* Jing Sun, Bin Zi, Wei Chen, and Yucheng Wu

Cite This: *ACS Nano* 2021, 15, 5294−5306

Read Online

ACCESS | Metrics & More | Article Recommendations | Supporting Information

ABSTRACT: Soft actuators and microrobots that can move spontaneously and continuously without artificial energy supply and intervention have great potential in industrial, environmental, and military applications, but still remain a challenge. Here, a bioinspired MXene-based bimorph actuator with an asymmetric layered microstructure is reported, which can harness natural sunlight to achieve directional self-locomotion. We fabricate a freestanding MXene film with an increased and asymmetric layered microstructure through the graft of coupling agents into the MXene nanosheets. Owing to the excellent photothermal effect of MXene nanosheets, increased interlayer spacing favoring intercalation/deintercalation of water molecules and its caused reversible volume change, and the asymmetric microstructure, this film exhibits light-driven deformation with a macroscopic and fast response. Based on it, a soft bimorph actuator with ultrahigh response to solar energy is fabricated, showing natural sunlight-driven actuation with ultralarge amplitude and fast response (346° in 1 s). By utilizing continuous bending deformation of the bimorph actuator in response to the change of natural sunlight intensity and biomimetic design of an inchworm to rectify the repeated bending deformation, an inchwormlike soft robot is constructed, achieving directional self-locomotion without any artificial energy and control. Moreover, soft arms for lifting objects driven by natural sunlight and wearable smart ornaments that are combined with clothing and produce three-dimensional deformation under natural sunlight are also developed. These results provide a strategy for developing natural sunlight-driven soft actuators and reveal great application prospects of this photoactuator in sunlight-driven soft biomimetic robots, intelligent solar-energy-driven devices in space, and wearable clothing.

KEYWORDS: *soft actuator, sunlight-driven actuation, photoactuator, self-locomotion, soft robot*

Soft untethered microrobots that can move without artificial energy supply and control have great potential in industrial, environmental, and military applications but still remain a big challenge. Among them, one of the key factors is to develop soft actuators that can harness environmental natural energy. In this respect, nature has provided us the inspiration. Many plants and animals in nature have evolved the capability of responding to the change of environmental stimuli (*e.g.*, natural sunlight, ambient humidity, and earth's magnetic field) and producing corresponding mechanical motions. For example, young sunflowers can track the sun's movement because of the asymmetric elongation on opposite sides of stems from the solar irradiation;[1] pine cone scales bend to release the ripe seeds in dry ambient air and close in wet conditions due to the migration of water molecules inside the aligned microstructures,[2] and *Drosophila melanogaster* can sense and fly toward a light source to produce phototactic motion.[3] Inspired by these living organisms with intelligent stimuli-response features, soft actuators for generating mechanical deformation under external energy stimulation have been greatly developed, which have received enormous interests in the fields of soft robotics, artificial muscle, smart wearable clothing, and MEMS.[4−17] Among various types, actuators driven by light have emerged as one of the most

Received: December 24, 2020
Accepted: February 23, 2021
Published: March 2, 2021

https://dx.doi.org/10.1021/acsnano.0c10797
ACS Nano 2021, 15, 5294−5306

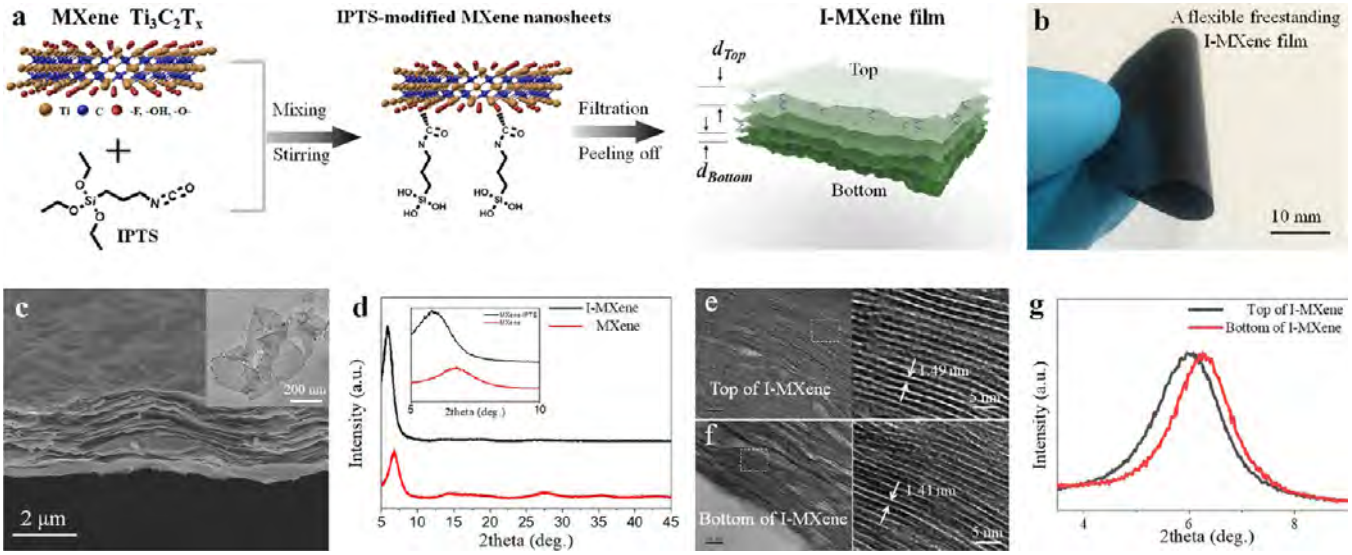

Figure 1. Fabrication and characterization of the I-MXene film. (a) Schematic diagram for the fabrication of I-MXene film. (b) Optical image of the bending of the freestanding I-MXene film. (c) Cross-sectional SEM image of the I-MXene film. The inset is a TEM image of the MXene nanosheets. (d) XRD patterns of the I-MXene film and MXene film. The inset is a magnified XRD pattern. (e, f) High-resolution cross-sectional TEM images of the top and bottom regions of the I-MXene film, respectively. (g) Comparison for the XRD patterns of the top and bottom of the I-MXene film.

attractive actuators owing to the advantageous features of untethered actuation, no contact, concise control, and rich sources (*e.g.*, endless sunlight).[18−26] However, most of the reported photoactuators need to use artificial light energy supply (*e.g.*, xenon light, LED, or laser) and generate continuous deformation by artificial control of the on/off switching of the light irradiation. These may greatly increase the complexity of the actuation system and limit its miniaturization and further application range. Therefore, it is significant to design soft actuators and related microrobots that can harness natural sunlight and generate designed continuous locomotion.

To achieve directional locomotion driven by natural sunlight, several aspects need to be considered. One aspect is to fabricate soft actuators that generate continuous repeated motion under natural sunlight, and the other is the robot configuration design for regulating repeated motion into the locomotion in a desired direction.[11] Just as the motions of living organisms (*e.g.*, pine cones and sunflowers) are derived from the reversible shape change of the aligned microstructures under environmental stimulation,[1,2] the actuator performance is intensely affected by the microstructures and their reversible deformation. Carbon nanomaterials, such as one-dimensional (1D) carbon nanotubes and two-dimensional (2D) graphene with excellent optical and mechanical properties and ideal structure assembly features, have been widely used to prepare photoactuators with layered or network microstructures, which exhibit high-performance actuation and promising applications in soft robotics.[27−35] For instance, Wang *et al.* reported a somatosensory light-driven robot capable of integrated perception and motility, in which the polydopamine-reduced graphene oxide is used as one of the core active materials to enable light actuation.[35] However, it is still difficult to achieve large deformation as well as directional locomotion under natural sunlight for the studied nanocarbon-based photoactuators and soft robots. Therefore, developing promising light-responsive materials and ideal microstructures that can exceed the performance of currently used materials is highly desirable.[36]

Recently, MXene, a type of 2D transition metal carbide and/or nitride, has attracted great research interests recently by virtue of excellent properties and promising applications in energy storage and conversion, sensing, electromagnetic wave shielding, biomedicine, and so on.[37−40] Among numerous types of MXenes, $Ti_3C_2T_x$ is the most widely studied MXene material. In particular, $Ti_3C_2T_x$ has shown high light absorption across a broad range of wavelengths and an outstanding internal photothermal conversion capability (efficiency of ∼100%),[41,42] 2D layered structure favored for the intercalation and deintercalation of ions and water molecules,[43] and abundance of surface hydrophilic functional groups, which shows potential for the construction of high-performance soft actuators.[44−48] For instance, Cai *et al.* integrated cellulose nanofibers into $Ti_3C_2T_x$ MXene nanosheets to form an MXene−celloluse composite and combined it with polycarbonate film to develop a bilayer soft actuator that produces large bending deformation (angle change ∼169°) driven by artificial near-infrared (NIR) light.[47] However, in addition to combining with other materials to achieve light-driven deformation, there is a lack of research on the photomechanical deformation characteristics of pure MXene films, which is significant for the improvement of the light-driven actuation performance. Moreover, MXene-based actuators driven by natural sunlight as well as directional locomotion without artificial control are still not realized up to now. Therefore, the exploitation of various MXene materials with an elaborately designed microstructure and excellent light-responsive performance and their derived natural sunlight-driven actuators and microrobots are still promising.

In this paper, an MXene-based bimorph actuator with an enlarged and asymmetric microstructure is designed, which harnesses natural sunlight and achieves directional self-locomotion through the biomimetic design. A freestanding MXene film with increased interlayer spacing, asymmetric layered microstructure, and enhanced mechanical properties is

https://dx.doi.org/10.1021/acsnano.0c10797
ACS Nano 2021, 15, 5294−5306

fabricated through the intercalation of a coupling agent 3-isocyanatopropyltriethoxysilane (IPTS) into the MXene nanosheets. This freestanding film shows reversible bending deformation with macroscopic amplitude and fast response (3 mm in 0.6s) to the light, which is attributed to the excellent photothermal effect of MXene, increased interlayer spacing favoring intercalation/deintercalation of water molecules and its caused reversible volume change, and the asymmetric microstructure for amplification of the microdeformation. Based on it, a soft bimorph actuator with ultrahigh response to natural sunlight is fabricated, showing natural sunlight-driven actuation in the ambient environment with outstanding performance (346° in 1 s). When the incident light intensity is increased to 200 mW/cm^2, the actuator outputs an ultralarge deformation (~700° in 2.1s) which exceeds the performance of most of the reported soft photoactuators. By utilizing continuous repeated bending deformation of the bimorph actuator in response to natural sunlight fluctuation and a biomimetic "inchworm" design to rectify the repeated bending deformation, an inchwormlike soft robot is constructed to locomote spontaneously and directionally without artificial energy and control. It can also transport an object and be disguised as a real inchworm to crawl in the wild environment. Moreover, soft arms for lifting objects and a "panda" robot that can change facial expression and body movements from depressed and huddled to happy dancing in the natural sunlight are also constructed. In terms of intelligent wearable applications, wearable ornaments and brand logos that can integrate with clothes and produce three-dimensional (3D) deformation under natural sunlight to protect the skin from strong sunlight and make clothes more intelligent are also designed. Compared to previous work about MXene actuators,[47,48] we have not only designed a freestanding MXene film with increased and asymmetric interlayer spacing that can generate visible macroscopic light-driven deformation but also realized this asymmetric microstructural MXene-based actuator with ultrahigh response to solar energy and its spontaneously directional self-locomotion under natural sunlight. These results provide insight for designing natural sunlight-driven actuators and reveal the potential applications of the intelligent bimorph photoactuator in sunlight-driven biomimetic soft microrobots, self-deployable sun sails in space, smart sun visors in space, intelligent solar energy devices, and wearable clothing.

RESULTS AND DISCUSSION

The freestanding MXene film with an enlarged as well as asymmetric layered microstructure was prepared by IPTS modification and subsequent solution filtration, as shown in Figure 1a. The MXene ($Ti_3C_2T_x$) was fabricated by the clay method. A Tyndall scattering effect was observed in the colloid solution of exfoliated MXene nanosheets, which indicates the good dispersion (Figure S1). IPTS, a coupling agent with isocyanate, shows excellent performance in the surface modification of the organic and inorganic materials, improving their mechanical properties.[49,50] Here, the purpose of using IPTS is to enlarge the interlayer spacing of the stacked MXene film and at the same time improve the mechanical flexibility. The IPTS solution is hydrolyzed first, with ethoxyl end groups removed. Then, the hydrolyzed IPTS is added into MXene−EtOH solution to modify the MXene nanosheets. The hydroxyl group of MXene is grafted with the −NCO groups, forming IPTS-modified MXene nanosheets.[51,52] Afterward, by the vacuum filtration method, IPTS-modified MXene (I-MXene) film is obtained. As a result of the great interaction between the MXene and IPTS, the filtrated I-MXene film can be easily peeled off to form a freestanding film with an excellent mechanical property. As shown in Figure 1b and Movie S1, this I-MXene film is highly flexible and compliant, which is suitable for constructing large-deformation soft actuators. The stress−strain curves (Figure S2) show the high tensile strength (~140 MPa) of the freestanding I-MXene film, which is greatly enhanced compared to the pure MXene film without IPTS modification. Figure 1c and Figure S3 show the cross-sectional SEM images of the obtained I-MXene film, indicating the loosely lamellar structure. The inset TEM image indicates that the lateral size of the MXene nanosheets is between 200 and 500 nm. The X-ray diffraction (XRD) pattern of I-MXene film is also measured to investigate the layered microstructure (Figure 1d). It can be seen that the characteristic diffraction peak corresponding to the (002) crystal plane of MXene in I-MXene film is shifted to 5.9° compared with that of the pure MXene film (6.8°), indicating the increase of the interlayer spacing in the stacked MXene nanosheets through the intercalation of IPTS.

In order to validate that IPTS is successfully grafted onto the MXene nanosheets, the FTIR spectra of the as-prepared I-MXene (black curve) and pure MXene (red curve) are measured, as shown in Figure S4. In contrast to the pure MXene, the peak intensity of 3400 and 1630 cm^{-1} in the FTIR spectra of I-MXene apparently decreases, indicating that the hydroxyl groups on the MXene nanosheets are occupied and participated in the grafting reaction. Meanwhile, the weak peaks at 882 and 1090 cm^{-1} in I-MXene correspond to the vibration peak of —Si—OH and —Si—O—, respectively, indicating the existence of the IPTS in the films. There is an obvious peak at 1450 cm^{-1} in I-MXene, which corresponds to that of the R—COO— group. It is worth noting that the peak at 2400 cm^{-1} corresponding to —N═C═O in IPTS does not appear in the I-MXene, revealing that IPTS and MXene are not simply mixed. Reactions occurred between —N═C═O and —OH on the MXene surface, forming —COO— groups.[53]

Besides the increased interlayer spacing and the enhanced mechanical properties, the I-MXene film also possesses an asymmetric microstructure. Figure S5 gives the SEM images of the top and bottom surfaces of the I-MXene film, respectively. It is clearly seen that the wrinkles on the bottom surface adjacent to the filter paper are greater in number and smaller than on the top surface exposed to air. This morphology difference is consistent with the observation from the AFM images (Figure S6). In order to verify the asymmetric microstructure, Figure 1e,f gives the high-resolution cross-sectional TEM (HRTEM) images of the top and bottom regions of the I-MXene film. The top region of the I-MXene film has a crystal lattice fringe with an interlayer spacing of 1.49 nm, while the bottom region shows an interlayer spacing of 1.41 nm. Moreover, XRD patterns at the top and bottom of the I-MXene film are also investigated. As given in Figure 1g, the (002) diffraction peaks from the top and bottom are, respectively, located at 5.9° and 6.3°, further confirming that the I-MXene film has asymmetric interlayer spacing in the top and bottom of the film. In addition, the hydrophilicity of the top and bottom surfaces of the I-MXene film is also measured (Figure S7). Both surfaces show good hydrophilicity, and the water contact angle on the top surface is smaller, indicating the asymmetric hydrophilicity. Here, the formation of this

https://dx.doi.org/10.1021/acsnano.0c10797
ACS Nano 2021, 15, 5294−5306

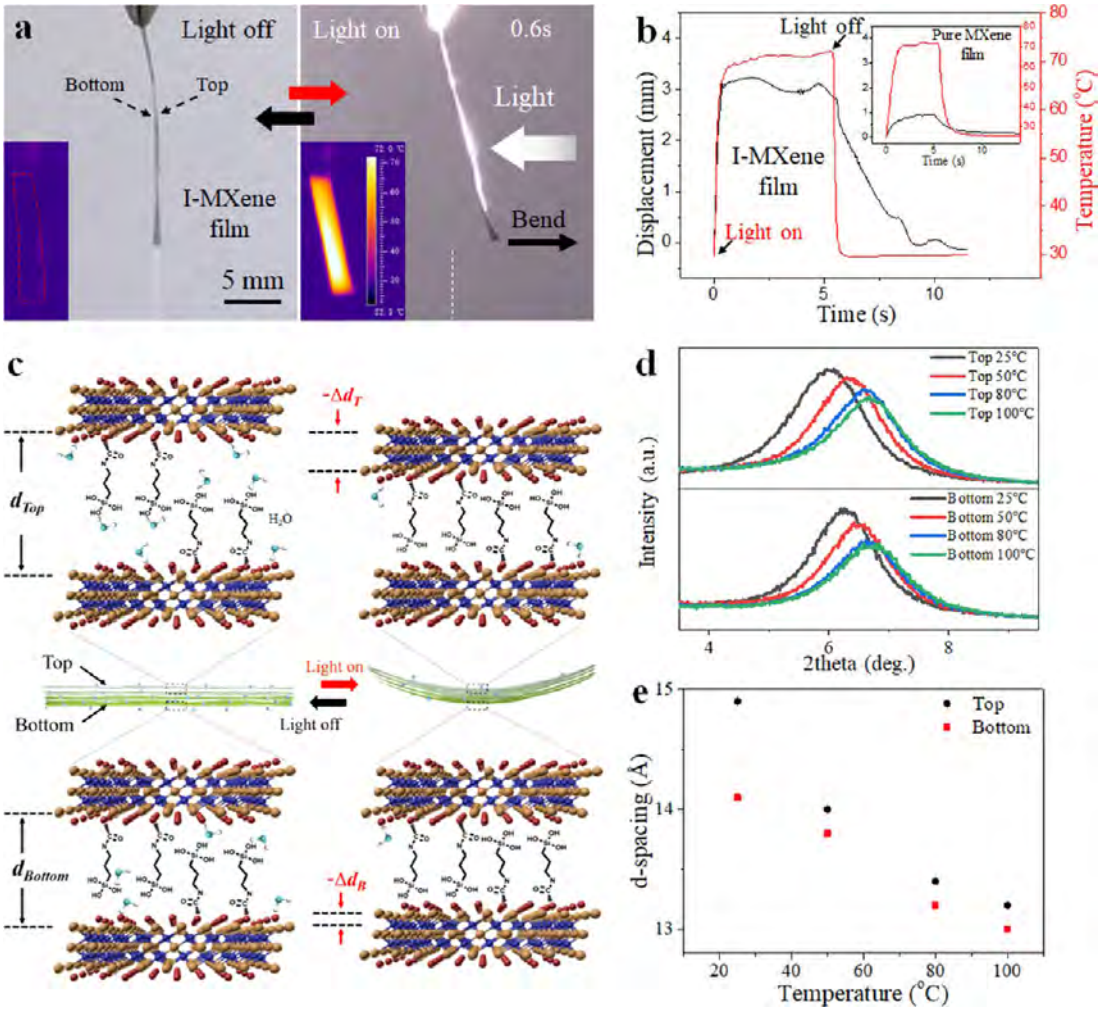

Figure 2. Light-driven deformation of the freestanding I-MXene film with asymmetric microstructure. (a) Optical images of the reversible deformation for the freestanding single I-MXene film under simulated sunlight irradiation (265 mW/cm^2). The light is incident from the right side. The insets are the corresponding infrared thermal images. (b) Displacement of the I-MXene film tip under the light stimulation and its simultaneous temperature variation. The inset shows the actuated displacement and temperature variation of the freestanding pure MXene film under light irradiation. (c) Schematic diagram showing the mechanism of the light-driven deformation for the I-MXene film. (d) XRD patterns from the top and bottom of the I-MXene film under different temperatures. (e) Interlayer *d*-spacing of the top and bottom of the I-MXene film as a function of the temperature.

asymmetric film with different interlayer spacing may be attributed to the pressure gradient change in the assembly of the MXene nanosheets during the filtration process. In the vacuum filtration process, the deposited MXene nanosheets at the bottom endure a higher filtration pressure, which induces a denser structure and a smaller interlayer spacing of the bottom layer. With the continuous deposition of the nanosheets on the filter membrane, the pressure on the upper layer decreases correspondingly, leading to the relatively loose structure of the upper layer and an increase of the interlayer spacing. In the meantime, compared with the top layer, the bottom MXene layer suffers the filtration pressure for a longer time, which also contributes to a smaller interlayer spacing. Besides, a similar phenomenon has also been observed in some reports.[54−56] In order to further confirm this phenomenon, the pure MXene film without any modification is also prepared by the same method, and the microstructure of the top and bottom is also characterized by HRTEM and XRD. As shown in Figure S8a,b, the interlayer spacing in the top of the unmodified pure MXene film is different from that in the bottom. The XRD patterns (Figure S8c) also reveal that the interlayer spacing decreases from the top to the bottom of the pure MXene film, which is consistent with the trends of I-MXene film.

This freestanding I-MXene film can produce macroscopic reversible bending deformation with a fast response when exposed to light irradiation. As shown in Figure 2a, when the light is incident from the right side, the freestanding I-MXene film generates bending deformation with the bending direction toward the top surface and bending displacement of about 3 mm in 0.6 s. After the light irradiation is turned off, it recovers to the original state within 3.8 s (Movie S2). The corresponding infrared thermal images in the insets of Figure 2a show that the temperature of the film increases with the deformation (Movie S3). Figure 2b gives the detailed bending displacement change of the film as well as the simultaneous temperature variation during the light-driven actuation process. The temperature variation is nearly consistent with the displacement change, indicating that the deformation is related to the temperature change. The light-driven deformation of the freestanding I-MXene film with different incident direction is

https://dx.doi.org/10.1021/acsnano.0c10797
ACS Nano 2021, 15, 5294−5306

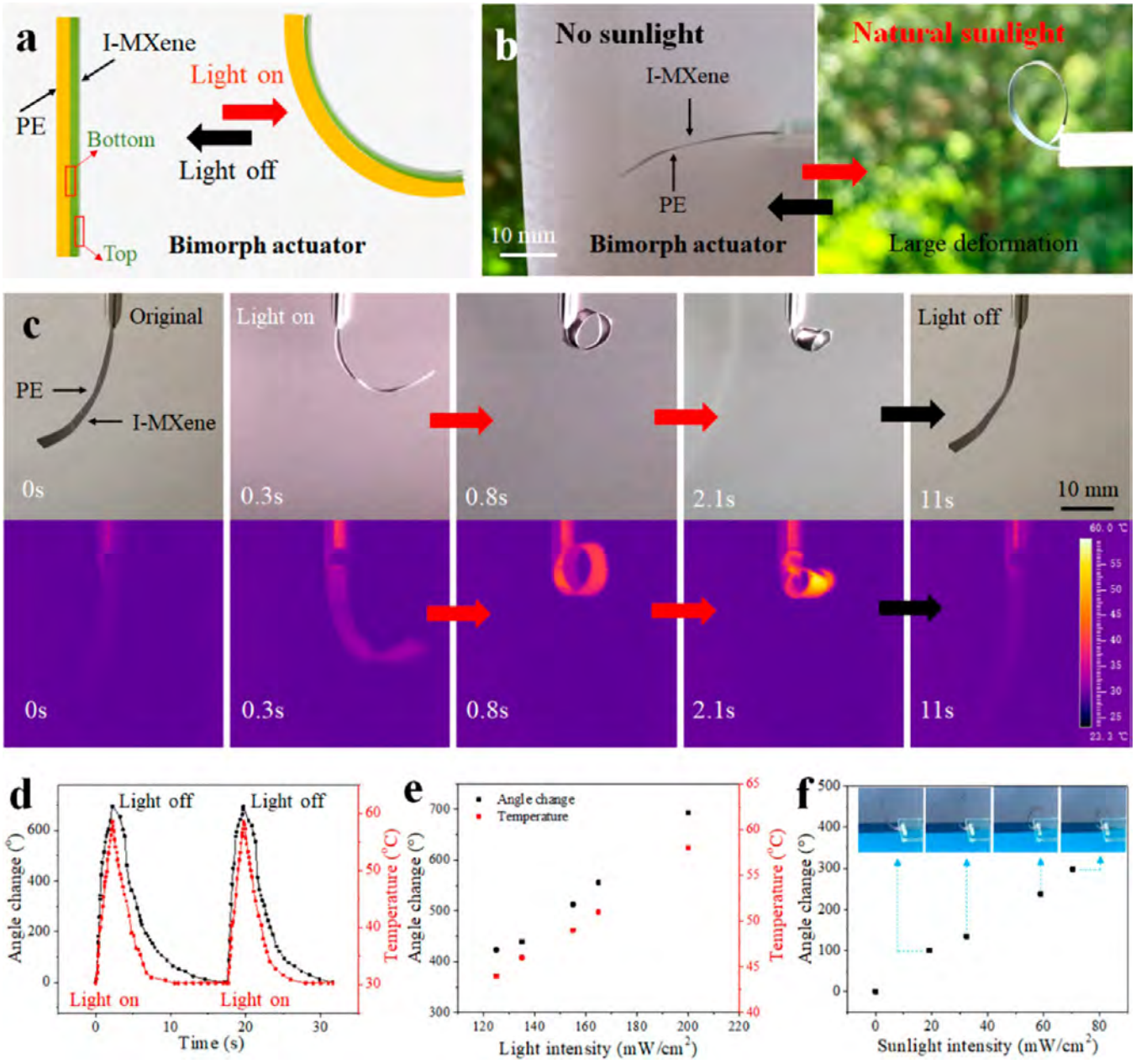

Figure 3. Natural sunlight-driven actuation of the bimorph actuator. (a) Schematic diagram of the I-MXene/PE bimorph actuator. (b) Optical images of reversible bending deformation of the bimorph actuator exposed to the natural sunlight irradiation. (c) Optical images and infrared thermal images of the light-driven actuation of the bimorph actuator. (d) Bending angle change and the simultaneous temperature variation of the bimorph actuator under light irradiation. (e) Maximal angle change and temperature variation of the bimorph actuator as a function of light intensity. (f) Natural sunlight-driven angle change of the bimorph actuator with different sunlight intensity. The insets are the corresponding optical images of the natural sunlight-driven deformation.

also measured (Figure S9). When the film is irradiated from the left side, it still bends toward the top surface, revealing that its deformation is independent of the incident light direction. Furthermore, the bending displacement can be reduced with the decrease of the light intensity (Figure S10). Besides the I-MXene film, the deformation of freestanding pure MXene film under the same stimulation condition is also investigated for comparison. As shown in the inset of Figure 2b and Figure S11, the pure MXene film also bends to the top surface after exposed to the light irradiation, accompanied by the temperature variation. However, the generated bending displacement (0.9 mm) is smaller than the displacement of the I-MXene film, indicating the improved actuation performance through the IPTS modification.

The mechanism for the light-driven deformation of the freestanding I-MXene film is deduced in Figure 2c. It is well-known that MXene nanosheets have excellent hydrophilicity and can adsorb water molecules through hydrogen bonding between surface groups and water molecules, and the interaction is reversible.[43] Meanwhile, the modification of MXene with the grafted IPTS provides a favorable increased interlayer spacing for the fast intercalation/deintercalation of more water molecules. Moreover, the MXene nanosheet is also excellent at absorbing light and converting it to heat. When the light is irradiated on the I-MXene film, the fast loss of adsorbed

https://dx.doi.org/10.1021/acsnano.0c10797
ACS Nano 2021, 15, 5294−5306

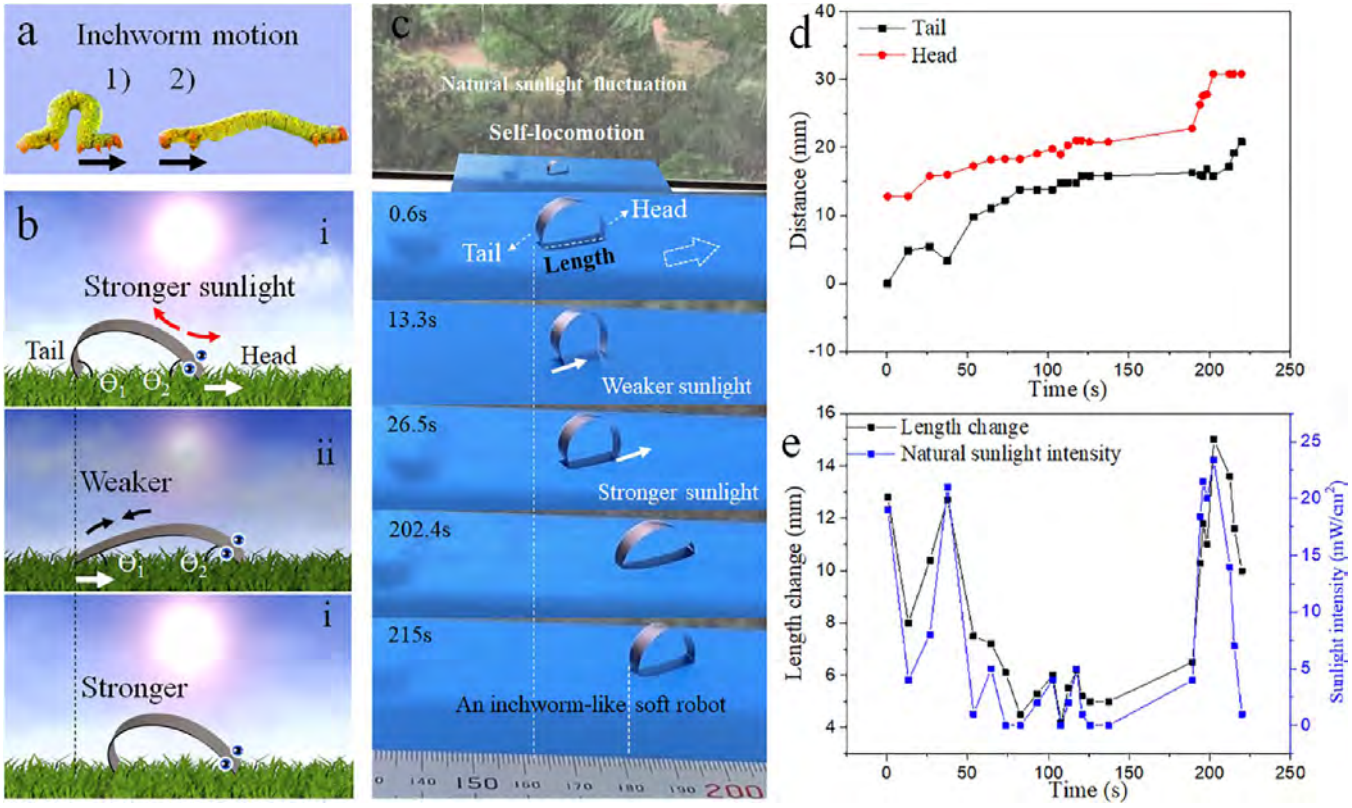

Figure 4. Self-locomotion driven by ambient natural sunlight fluctuation. (a) Schematic diagram of the inchworm motion with head and tail alternately moving forward. (b) Schematic of the design of the inchwormlike soft robot with continuous directional crawling motion driven by natural sunlight fluctuation. (c) Optical images of the directional self-locomotion for the inchwormlike soft robot driven by natural sunlight fluctuation. This robot can continuously crawl forward for 19 mm in 215 s without artificial control. (d) Crawling distance of the robot's head and tail under natural sunlight irradiation as a function of time. (e) Length change of the soft robot (black curve) and the corresponding real-time fluctuation of the incident natural sunlight intensity (blue curve) with change in time.

water molecules occurs due to the excellent photothermal property of MXene nanosheets, leading to the decrease of interlayer *d*-spacing and thus the contraction deformation of the film.[57] Because of the asymmetric interlayer spacing, the contraction of the top may be greater than that of the bottom, resulting in the bending deformation of the whole film with the bending direction toward the top surface. After the light source is turned off, the film reabsorbs the surrounding water molecules and returns to the original shape. In order to validate the mechanism, the interlayer *d*-spacing at the top and bottom of I-MXene film with different temperatures is measured by XRD, as shown in Figure 2d. With the increase of temperature, both of the (002) diffraction peaks from the top and bottom are shifted to the right, indicating the decrease of the *d*-spacing due to the desorption of water molecules in the interlayers. Figure 2e shows the temperature dependence of the *d*-spacing of the top and bottom of the I-MXene film. It can be seen that the change of *d*-spacing at the top is greater than that at the bottom. When the temperature increases from 25 to 100 °C, the *d*-spacing at the top decreases from 14.9 to 13.2 Å, while that at the bottom decreases from 14.1 to 13.0 Å, confirming that the bending deformation is induced by the asymmetric *d*-spacing change between the top and bottom. Furthermore, the actuation of the freestanding I-MXene film in different humidity environments is also studied (Figure S12). With the increase of the relative humidity (RH), the I-MXene film bends toward its bottom surface, which is opposite to the direction of light-driven deformation. This further reveals that the top of the I-MXene film with larger *d*-spacing and better hydrophilicity can absorb more water molecules, leading to the larger swelling compared with that of the bottom.

Owing to the excellent light-driven deformation, the I-MXene film can be used as a promising component to further construct natural sunlight-driven high-performance photoactuators. As shown in Figure 3a, the actuator is composed of an I-MXene/polyethylene (PE) bimorph structure. Here, a bimorph structure is employed because it could generate bending motion by using the deformation mismatch between the two layers, which can maximize the actuation performance of the I-MXene film. As we know, PE is a commercially used polymer material with large coefficient of thermal expansion (about 500×10^{-6}/°C).[7] The bimorph actuator is constructed by attaching the bottom surface of the I-MXene film to the PE film, in which the output bending deformation can be maximized. Under light irradiation, the I-MXene film generates contraction-induced bending deformation. Meanwhile, it absorbs light and converts it into thermal energy to heat the PE film, causing the thermal expansion of the PE film. Because of the bimorph structure, a large bending deformation can be achieved for this actuator. The bimorph actuator exhibits an excellent light-driven actuation performance and can be directly driven by natural sunlight. As shown in Figure 3b, when the actuator is placed in the natural environment, under the illumination of natural sunlight (80 mW/cm^2), it generates bending deformation with the bending angle up to 346°.

https://dx.doi.org/10.1021/acsnano.0c10797
ACS Nano 2021, 15, 5294−5306

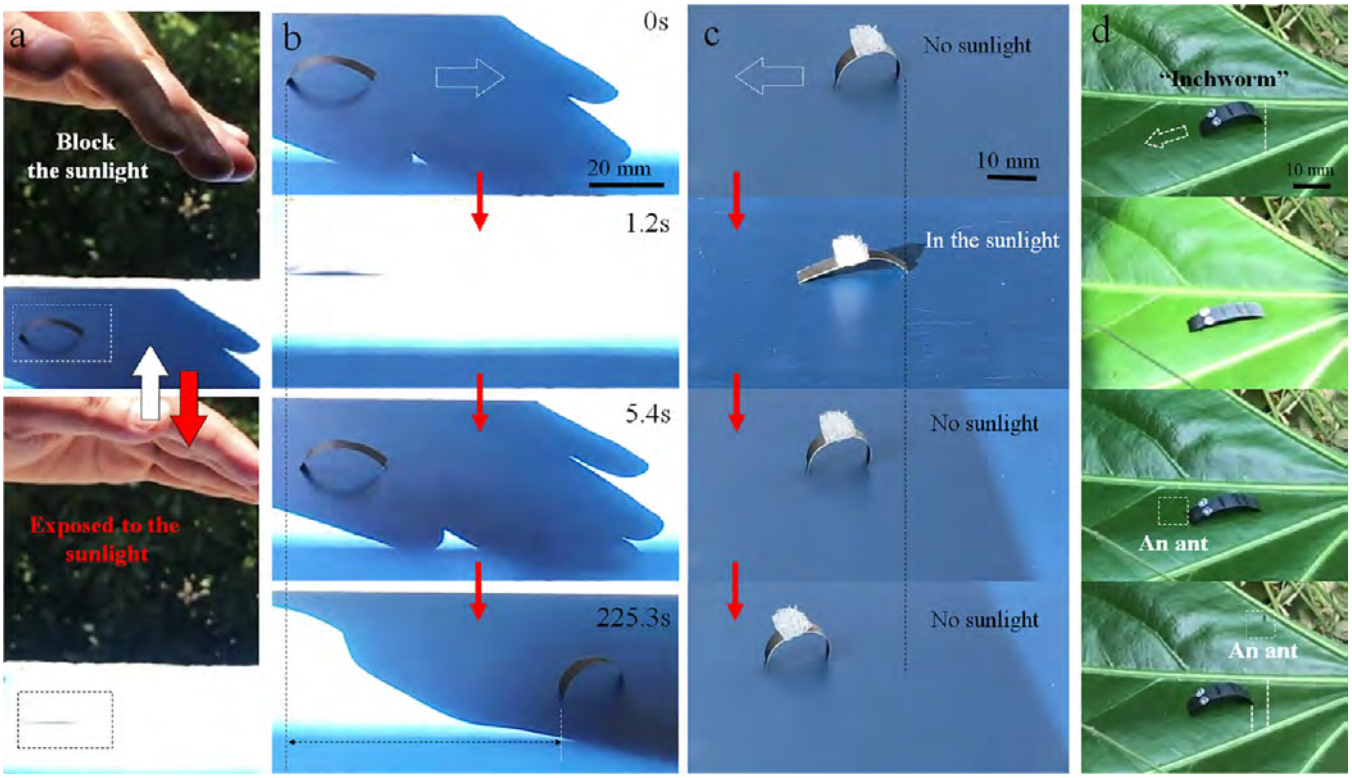

Figure 5. Natural sunlight-driven locomotion controlled by the human hand. (a) Optical images showing the reversible natural sunlight-driven deformation of this robot by blocking/unblocking the incident sunlight with the human hand. (b) Natural sunlight-driven locomotion controlled by the human hand. (c) Transportation of an object by the robot driven by natural sunlight. (d) Directional crawling of a biomimetic "inchworm" robot on a fallen leaf driven by natural sunlight in the wild environment. In the crawling process, an ant appears on this leaf and comes into contact with the "inchworm".

For the purpose of quantitatively analyzing the light-driven actuation, simulated sunlight instead of natural sunlight is employed as the light stimulus to stimulate the bimorph actuator. As shown in Figure 3c, under the light irradiation (200 mW/cm^2), the bimorph actuator bends into a circle in 0.8 s. After continuous irradiation for 2.1 s, the bending angle can reach as large as nearly 700°. After turning off the light source, the actuator returns to its original shape in 11 s, indicating the good reversibility (Movie S4). The corresponding infrared thermal images of the actuation process are also provided in Figure 3c, showing the photothermal-effect-induced deformation (Movie S5). Under two cycles of light stimulation, the change of bending angle is consistent with the corresponding temperature variation (Figure 3d), further confirming the photothermal mechanism. The light-driven deformations with different light intensities are also measured, as shown in Figure 3e. With the decrease of the incident light intensity, both the bending angle and temperature of the bimorph actuator reduce linearly, indicating the good controllability of this bimorph actuator. Long time stability of the light-driven actuation is also examined (Figure S13). Under the cyclic light irradiation for about 500 cycles, the maximal bending angle change keeps stable without obvious change. Moreover, the weight change of the bimorph actuator during light-driven actuation is also investigated (Figure S14). The weight of the actuator is reduced by 1.5 wt % (0.25 mg) under light irradiation for 6 s, indicating the release of water molecules in this actuation process. After light irradiation is turned off, the weight quickly returns to the initial weight within 10 s in the ambient air condition, further confirming the fast actuation response. We also compare the performance of our actuator with that of other reported photoactuators, as shown in Figure S15. Our I-MXene-based actuator exhibits outstanding performance in terms of deformation angle and the response time.

The deformation of the bimorph actuator under the irradiation of natural sunlight is also studied, as shown in Figure 3f and Movie S6. With the variation of the ambient natural sunlight intensity, the bending deformation angle of the actuator changes accordingly. This result proves that the actuator can produce significant continuous deformation in response to the natural sunlight due to the fact the intensity of natural sunlight in the ambient environment usually fluctuates and does not remain constant, offering a foundation for the construction of a natural sunlight-driven soft robot with continuous self-locomotion. Furthermore, in terms of the actuator shape design, in addition to the flattened shape, we can also adjust the initial shape of the actuator by using the heat setting process,[58] so as to prepare the bent-shaped, circular-shaped, and S-shaped actuator, which can realize the reversible deformation from upward bending to downward bending, from circular to straight, and from S-shape to straight under the natural sunlight irradiation (Figure S16). This is also very useful for the construction of soft robots with different shapes.

By taking the ambient natural sunlight as the energy source and simulating the crawling motion of the inchworm, we further designed a biomimetic soft robot based on the bimorph actuator, which can locomote spontaneously and directionally (Figure 4). The inchworm is a kind of soft invertebrate in

https://dx.doi.org/10.1021/acsnano.0c10797
ACS Nano 2021, 15, 5294−5306

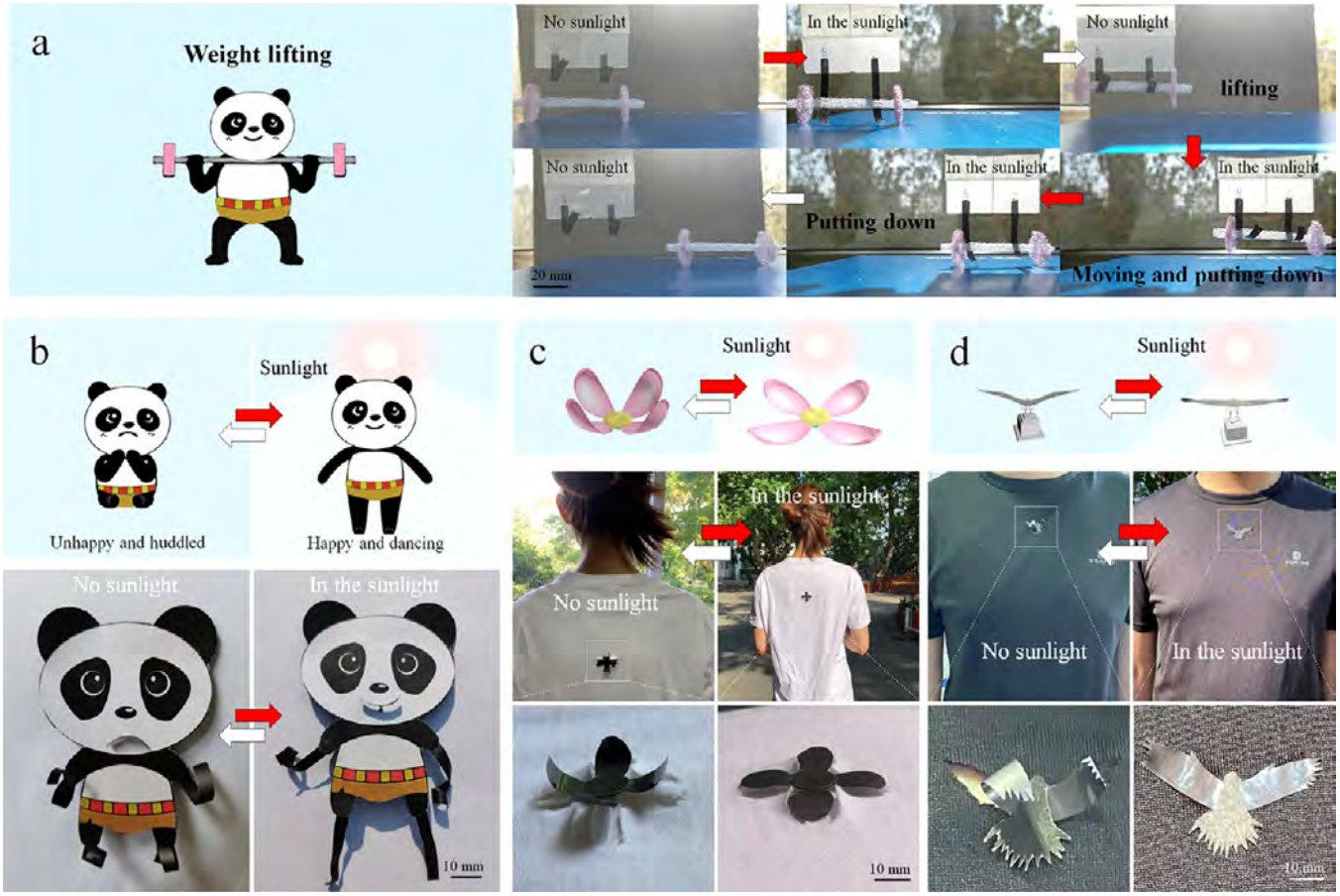

Figure 6. Natural sunlight-driven soft robot and wearable ornaments. (a) Weight lifting performance of the soft arms driven by natural sunlight. (b) Schematic diagram as well as optical images of reversible deformation of the "panda" robot from an unhappy and huddled state to happy and dancing state with natural sunlight off and on. (c) Schematic and optical images of reversible blooming of the wearable artificial lilac flower in the sunlight. (d) Schematic and optical images showing the wearable eagle ornament spreading its wings in the sunlight and folding them without sunlight.

nature with a distinctive way of crawling. It uses the stretching and contraction of the back muscle to realize the directional crawling motion. As shown in Figure 4a, the inchworm's crawling process can be simply divided into two ways: (1) the tail is fixed, and the body is stretched to drive the head forward; (2) the head is fixed, and the body is arched to drive the tail to move forward. Through the alternate motion of stretching and bending, the inchworm realizes the directional crawling. By mimicking the principle of this crawling, we design an inchwormlike soft robot that can crawl directionally and continuously by making use of the fluctuation of natural sunlight. As shown in Figure 4b, the soft robot has an original asymmetric curved shape through the heat setting process. The angles between the head (right) and tail (left) of the robot and the ground are named as θ_2 and θ_1, respectively, and $\theta_1 > \theta_2$ at the initial status without sunlight irradiation. The robot takes the natural sunlight as the energy source and generates continuously spontaneous motion driven by the fluctuation of natural sunlight in the ambient environment. As we know, the sunlight irradiated on the ground can be affected by the natural environmental factors such as clouds, trees, and illumination angle. Therefore, natural sunlight intensity is not a fixed value but fluctuates in a certain range. This ambient sunlight fluctuation can be used as a natural energy source to realize the continuous directional locomotion of the robot without additional control. When the sunlight becomes stronger, the robot with the original curved shape bends upward to become stretched. The friction between the tail and the ground is greater than the friction between the head and the ground due to $\theta_1 > \theta_2$, which leads to the head stretching forward to the right side while the tail remains stationary (Figure 4bi). When the sunlight weakens, the robot bends downward to contract. Due to $\theta_1 < \theta_2$, the head of the robot stays fixed, and the tail shrinks to the right (Figure 4bii). Thus, a cycle of forward crawling motion of the soft robot is achieved. Under the fluctuation of ambient natural sunlight, this robot can continuously crawl forward, so as to realize directional locomotion. Figure 4c gives optical images of the self-locomotion for the inchwormlike soft robot driven by natural sunlight fluctuation. The robot is placed in the natural sunlight. When the sunlight intensity becomes weaker (13.3 s in Figure 4c), its tail moves to the right. As the sunlight intensity becomes stronger (26.5 s in Figure 4c), the head moves to the right. After being placed in the natural sunlight for 215 s, the robot crawls spontaneously to the right for about 19 mm (Movie S7). To the best of our knowledge, up to now, reports are still rare for the realization of the directional crawling motion of a soft robot driven by natural sunlight, without any extra artificial energy and control. Figure 4d shows the crawling distance of the robot's head and tail as a function of time, revealing the detailed process of the self-locomotion. The length change of the robot during the crawling process and the

https://dx.doi.org/10.1021/acsnano.0c10797
ACS Nano 2021, 15, 5294−5306

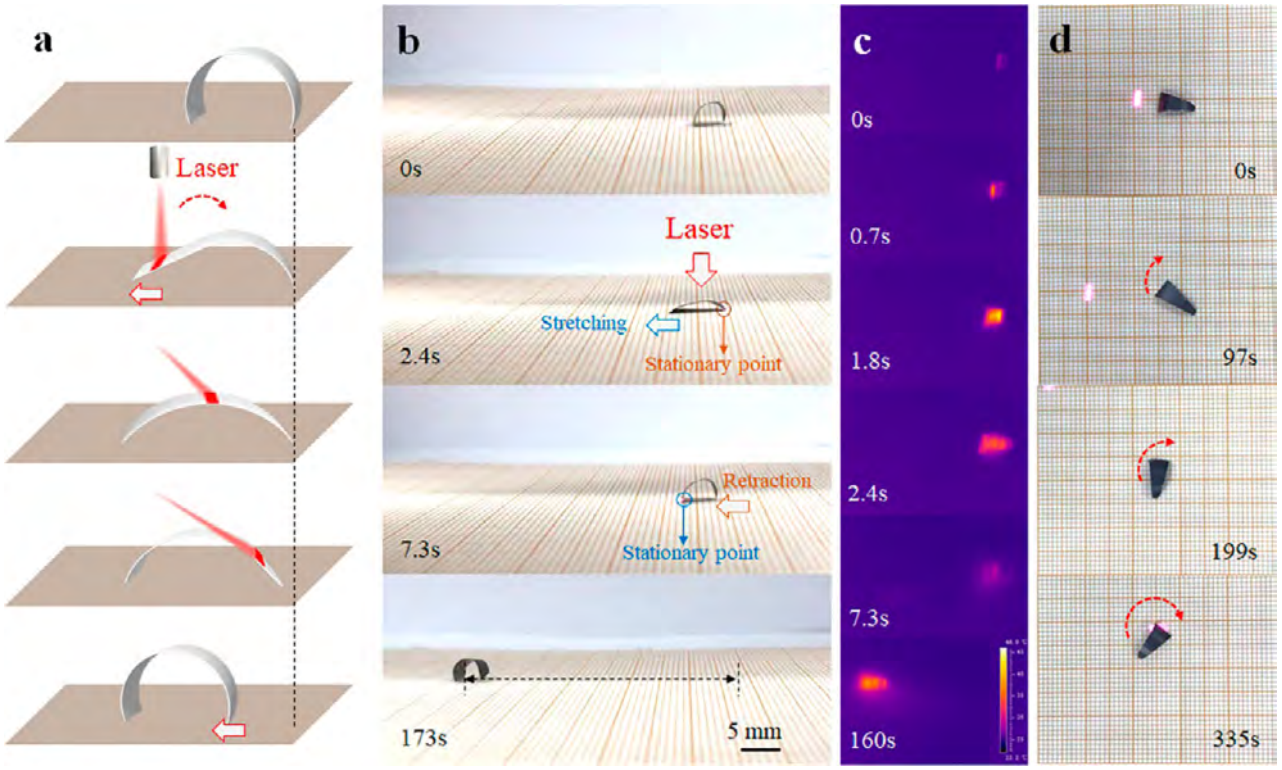

Figure 7. Continuous locomotion of the soft robot with controllable direction under laser irradiation. (a) Schematic diagram showing the continuous directional crawling motion of the soft robot controlled by cyclical laser scanning (from left to right). (b) Optical images of the directional crawling motion driven by the cyclical laser scanning (808 nm). (c) Infrared thermal images of the directional crawling motion. (d) Turning motion of the soft robot controlled by the laser.

corresponding fluctuation of the ambient natural sunlight intensity are also provided (Figure 4e). We can see that the fluctuation of the sunlight intensity is nearly consistent with the change of the robot's body length, which confirms that the robot's motion is caused by the natural fluctuation of incident sunlight.

Besides directly using ambient natural sunlight fluctuation, we can also control the deformation of the robot by using a human hand to cyclically block and unblock the natural sunlight, so as to achieve fast directional locomotion. As shown in Figure 5a, when the natural sunlight is blocked with the human hand, the robot is in the original curved shape. Once the hand is removed, the robot stretches into a straight shape under the natural sunlight irradiation. The cyclical deformation of the robot can be controlled through the repeated blocking/unblocking of the natural sunlight by the human hand; thus, the directional locomotion is realized (Figure 5b and Movie S8). Through this simple method of control, the robot crawls for a 73 mm displacement in 225 s. Besides the locomotion, the robot can also transport an object. As shown in Figure 5c and Movie S9, driven by natural sunlight, the robot can transport an object with a weight of 7.5 mg which is 1.7 times its own weight. Furthermore, a more realistic biomimetic "inchworm" robot that is disguised as a real inchworm is developed, and its sunlight-driven crawling on a fallen leaf in the wild environment is realized (Figure 5d and Figure S17). It is worth noting that, during the crawling process of the "inchworm", an ant appears on the leaf. The ant may be attracted by the "inchworm", crawls to the "inchworm", and makes contact with it (Movie S10).

Moreover, we further designed soft arms for weight lifting driven by natural sunlight, a "panda" robot that can change facial expression and body movements under natural sunlight irradiation, and wearable ornaments combined with clothes (Figure 6). Under natural sunlight, the soft arms with an original curled shape can bend downward to touch a plastic dumbbell (50 mg). After blocking the sunlight, it can lift the dumbbell that is 3 times heavier than its own weight (Figure 6a and Movie S11). Figure 6b shows the "panda" robot with mouth and limbs composed of the bimorph actuators. In the absence of sunlight, the robot is shown in an unhappy and huddled state. Once under the sunlight, it smiles and dances with all its limbs, showing a very happy state. Besides, a combination with fabric to develop intelligent wearable clothing is also an important application for the soft actuators. Here, the bimorph actuator can also be utilized to prepare wearable ornaments and brand logos that can generate 3D deformation in response to natural sunlight, which can prevent the skin from being exposed to strong sunlight as well as make our clothes more intelligent and fashionable. For example, we made an artificial lilac flower (Figure 6c) and integrated it with the T-shirt. When a person wearing it walks in the sun, the flowers on the clothes bloom automatically. An eagle ornament made of the bimorph actuator is attached to the front chest of a shirt and spreads its wings in the sunlight (Figure 6d).

In addition to natural sunlight, we also use an artificial light source (near-infrared laser) to realize the controllable crawling motion (directional and turning motion) of the soft robot (Figure 7). In order to make the robot more controllable, this crawling robot is designed to be a triangle shape, which can generate asymmetric friction at the front and back ends. As

https://dx.doi.org/10.1021/acsnano.0c10797
ACS Nano 2021, 15, 5294−5306

shown in Figure 7a, the triangular crawling robot is initially placed on the right side. Once the laser beam is controlled to scan the robot from left to right, the irradiated part of the robot produces stretching deformation. After the laser spot moves away, it recovers to the original bending shape. When the robot is cyclically scanned from left to right by the laser, it continuously crawls to the left side, with a distance of 73 mm in 173 s (Figure 7b and Movie S12). The infrared thermal images of this laser-controlled crawling motion are also provided in Figure 7c, revealing the precise control of the laser on the temperature and deformation of the irradiated part of the soft robot. Moreover, by dynamically changing the scanning direction of the laser beam on the robot, a turning motion with a rotation angle of 125° is also achieved (Figure 7d and Movie S13), which confirms the excellent controllability of the soft robot under laser stimulation. The mechanism of the light-driven rotation motion is further clarified (Figure S18). As shown in Figure S18a, the moving direction of the robot is controlled by the scanning path of the laser dot. In general, the head of the robot can be divided into two parts: the left wing and the right wing. When the left side is illuminated, it absorbs more heat than the right (phase 2), making the deformation of the left wing much greater than that of the right (phase 3). Then, after recovering, the moving direction of the actuator is changed (phase 4). Figure S18b shows the superimposed images of the turning motion of the soft robot, which further reveals this rotation process.

CONCLUSIONS

A freestanding I-MXene film with increased and asymmetric layered microstructure and enhanced mechanical properties is fabricated. It shows light-driven reversible deformation with macroscopic bending and a fast response (~3 mm in 0.6 s) mainly due to the excellent photothermal effect of MXene nanosheets, increased interlayer spacing favoring reversible volume change, and the asymmetric microstructure. Based on it, a soft bimorph actuator with ultrahigh response to solar energy is fabricated, showing a natural sunlight-driven outstanding actuation performance including large amplitude and fast response (346° in 1 s). By utilizing this high-performance bimorph actuator, together with the biomimetic design of the inchworm to rectify the locomotion, an inchwormlike soft robot is constructed to realize directional locomotion under ambient natural sunlight without any artificial control. Moreover, the soft robot can transport an object and be disguised as a real inchworm to crawl on a fallen leaf in the wild environment. Moreover, soft arms for a weight lifting performance driven by the natural sunlight, a "panda" robot that can change facial expression and body movements in the sunlight, and wearable smart ornaments that are combined with clothing and produce 3D deformation under natural sunlight are also developed. In comparison with the reported work, the innovation of this work lies in the following: (1) the design of a freestanding MXene film with increased and asymmetric interlayer spacing with a facile filtration method, and realization of its visible deformation under light irradiation; (2) the fabrication of the soft actuator based on the asymmetric microstructural MXene film, which shows an ultrahigh response to the light and outstanding actuation performance compared to many of the reported photo-actuators; (3) the achieving of multiform actuation of the actuator under natural sunlight, and even the spontaneously directional self-locomotion with no artificial energy and control. Therefore, this work not only provides a useful way for developing a soft actuator and robots driven by natural sunlight but also reveals the great prospect of this actuator in solar-energy-driven intelligent devices in space, wearable clothing, and next-generation sunlight-driven biomimetic soft microrobots.

EXPERIMENTAL SECTION

Materials. The precursor MAX was purchased from Forsman Scientific (Beijing) Co., Ltd. HCl was purchased from Shanghai Titan Scientific Co., Ltd. LiF and 3-isocyanatopropyltriethoxysilane (IPTS) were purchased from Sinopharm Chemical Reagent Co., Ltd. Acetic acid was purchased from Shanghai Lingfeng Chemical reagent Co., Ltd. PE films were purchased commercial products.

Fabrication of the I-MXene Film. MXenes ($Ti_3C_2T_x$) were prepared by the clay method, in which the Al layers in the MAX phase were selectively etched using LiF/HCl mixtures. First, 3 g of $Ti_3C_2T_x$ was added into 67 mL of HCl (6 M) containing 6 g of LiF. After being stirred at 60 °C for 48 h, the resultant product was washed with deionized water and centrifuged several times until the pH of the supernatant was above 6. Afterward, the dried sediments were dispersed in deionized water with a certain ratio and then ultrasonicated under an Ar_2 atmosphere for 2 h to exfoliate the MXene nanosheets. Centrifugation at 3500 rpm for 1 h was performed to remove the unexfoliated MXenes in the solution. The concentration of the obtained MXene solution was about 8 mg/mL. 25 mL of the obtained MXene solution was diluted with 165 mL of ethanol and stirred for 30 min for better dispersion. 210 mg of IPTS (95%) was dissolved in 10 mL of ethanol. Then, a few drops of acetic acid were added to promote the hydrolysis of IPTS until the pH of the mixture was between 4 and 5. After that, the IPTS−ethanol solution and the MXene−ethanol solution were transferred to a 500 mL three-necked round-bottom flask in sequence. After being stirred under an Ar_2 atmosphere for 24 h, the dispersion was washed with ethanol and then with deionized water and centrifuged 2−3 times to remove the redundant IPTS. After the last centrifugation, the sediments were dispersed in deionized water and stirred for 1 h. The concentration of the obtained IPTS-modified MXene solution was about 4 mg/mL. Then, the IPTS-modified MXene solution was filtrated to obtain the I-MXene film, and the thickness can be tuned by adjusting the volume of the filtrated I-MXene solution. Here, the I-MXene film with a thickness of about 2 μm is selected for the actuation measurement.

Fabrication of the Bimorph Actuator. The I-MXene/PE bimorph actuator was fabricated simply by directly pasting the adhesive PE film onto the top surface of the I-MXene film, and then cutting it into the predesigned shape for further treatment. Here, the thickness of the I-MXene film was about 2 μm, and the PE film with thickness of 40 μm was chosen. The bent-shaped actuator was prepared through the heat setting process. To be specific, the actuator was bent into the desired bending shape and fixed and then heated at 40 °C for 24 h. After being cooled down to room temperature, the actuator with a bending shape was obtained.

Characterizations and Measurements. The TEM images were obtained by a field-emission transmission electron microscope (JEM-2100F, JEOL). The HRTEM images were obtained by using a transmission electron microscope (JEM-1400, JEOL), and a focused ion beam electron beam double beam microanalysis system (Versa 3D, FEI) was used to prepare this ultrathin section sample. The XRD pattern was performed on an X-ray diffractometer with high-intensity graphite monochromatized Cu Kα radiation (Rigaku-TTR3). FTIR spectra were measured by a Fourier transform IR spectrometer (iN10 iZ10, Thermofisher). The SEM images were captured by a field-emission scanning electron microscope (SEM, SU8220, HITACHI). The AFM images were obtained by an atomic force microscope (NTEGRA, NT-MDT). The mechanical strength was measured by a high-precision electronic universal testing machine (CMT6103, MTS Systems). Simulated sunlight irradiation was provided by a xenon lamp (AULIGHT) equipped with the simulated sunlight filter. The

https://dx.doi.org/10.1021/acsnano.0c10797
ACS Nano 2021, 15, 5294−5306

displacement of the I-MXene film was measured by a laser displacement sensor (Keyence, LK-G80). The actuation performance of the bimorph actuator was recorded by digital camera, and the data of bending angle was obtained from the analysis of the camera recording. A thermal infrared imager (Fotric 225-1) was used to capture the infrared thermal images and record the temperature variation during light-driven actuation.

ASSOCIATED CONTENT

Supporting Information

The Supporting Information is available free of charge at https://pubs.acs.org/doi/10.1021/acsnano.0c10797.

Tyndall scattering effect of the MXene solution, stress−strain curves, SEM images, FTIR spectra, AFM image, water contact angles, HRTEM images, XRD patterns, light-driven deformation, maximal bending displacement, deformation of the I-MXene film in response to the RH change, cyclic light-driven actuation, real-time water change of the actuator, comparison of recently reported photoactuators, natural sunlight-driven actuation with different original shapes, optical image of the "inchworm" robot in the wild environment, and mechanism of the turning motion controlled by the laser (PDF)

Movie S1: Large bending deformation of the I-MXene film (AVI)

Movie S2: Light-driven actuation of freestanding I-MXene film (AVI)

Movie S3: Infrared video for the photoactuation of I-MXene film (AVI)

Movie S4: Photoactuation of the bimorph actuator (AVI)

Movie S5: Infrared video for the photoactuation of the bimorph actuator (AVI)

Movie S6: Natural sunlight-driven actuation of the bimorph actuator (AVI)

Movie S7: Continuous directional locomotion driven by natural sunlight fluctuation (AVI)

Movie S8: Directional crawling motion driven by natural sunlight (AVI)

Movie S9: Transportation by the robot driven by natural sunlight (AVI)

Movie S10: Crawling motion of "inchworm" in the wild (AVI)

Movie S11: Weight lifting of the soft arms (AVI)

Movie S12: Directional crawling motion driven by the laser (AVI)

Movie S13: Turning crawling motion driven by the laser (AVI)

AUTHOR INFORMATION

Corresponding Authors

Ying Hu − *Anhui Province Key Lab of Aerospace Structural Parts Forming Technology and Equipment, Institute of Industry & Equipment Technology and Key Laboratory of Advanced Functional Materials and Devices of Anhui Province, School of Materials Science and Engineering, Hefei University of Technology, Hefei 230009, P. R. China;* orcid.org/0000-0002-9711-6047; Email: huying@hfut.edu.cn

Ranran Wang − *State Key Laboratory of High Performance Ceramics and Superfine Microstructure, Shanghai Institute of Ceramics, Chinese Academy of Science, Shanghai 200050, P. R. China*; Email: wangranran@mail.sic.ac.cn

Guan Wu − *State Key Laboratory of Materials-Oriented Chemical Engineering, College of Chemical Engineering, Nanjing Tech University, Nanjing 211816, P. R. China;* orcid.org/0000-0002-0025-812X; Email: gwu2016@njtech.edu.cn

Authors

Lulu Yang − *Anhui Province Key Lab of Aerospace Structural Parts Forming Technology and Equipment, Institute of Industry & Equipment Technology, Hefei University of Technology, Hefei 230009, P. R. China*

Qiuyang Yan − *State Key Laboratory of High Performance Ceramics and Superfine Microstructure, Shanghai Institute of Ceramics, Chinese Academy of Science, Shanghai 200050, P. R. China; University of Chinese Academy of Sciences, Beijing 100049, P. R. China*

Qixiao Ji − *Anhui Province Key Lab of Aerospace Structural Parts Forming Technology and Equipment, Institute of Industry & Equipment Technology, Hefei University of Technology, Hefei 230009, P. R. China*

Longfei Chang − *Anhui Province Key Lab of Aerospace Structural Parts Forming Technology and Equipment, Institute of Industry & Equipment Technology, Hefei University of Technology, Hefei 230009, P. R. China*

Chenchu Zhang − *Anhui Province Key Lab of Aerospace Structural Parts Forming Technology and Equipment, Institute of Industry & Equipment Technology, Hefei University of Technology, Hefei 230009, P. R. China;* orcid.org/0000-0002-3433-598X

Jian Yan − *Key Laboratory of Advanced Functional Materials and Devices of Anhui Province, School of Materials Science and Engineering, Hefei University of Technology, Hefei 230009, P. R. China;* orcid.org/0000-0002-4486-712X

Lei Zhang − *Anhui Key Laboratory of Condensed Matter Physics at Extreme Conditions, High Magnetic Field Laboratory, Chinese Academy of Sciences, Hefei 230031, P. R. China*

Jing Sun − *State Key Laboratory of High Performance Ceramics and Superfine Microstructure, Shanghai Institute of Ceramics, Chinese Academy of Science, Shanghai 200050, P. R. China;* orcid.org/0000-0003-1101-1584

Bin Zi − *Anhui Province Key Lab of Aerospace Structural Parts Forming Technology and Equipment, Institute of Industry & Equipment Technology, Hefei University of Technology, Hefei 230009, P. R. China*

Wei Chen − *Research Centre for Smart Wearable Technology, Institute of Textiles and Clothing, The Hong Kong Polytechnic University, Hong Kong 999077, P. R. China;* orcid.org/0000-0001-9527-110X

Yucheng Wu − *Key Laboratory of Advanced Functional Materials and Devices of Anhui Province, School of Materials Science and Engineering, Hefei University of Technology, Hefei 230009, P. R. China*

Complete contact information is available at: https://pubs.acs.org/10.1021/acsnano.0c10797

Author Contributions

Y.H. planned and designed the project. Y.H. and L.Y. conducted the actuation experiments. R.W., Q.Y., Q.J. and J.S. helped to fabricate the materials. Q.Y., Q.J., R.W., L.C., C.Z., J.Y. and L.Z. helped to characterize the samples. J.Y., B.Z.,

https://dx.doi.org/10.1021/acsnano.0c10797
ACS Nano 2021, 15, 5294−5306

W.C. and Y.W. helped to elaborate the mechanism. Y.H., L.Y. and G.W. analyzed the data and wrote the paper. G.W., B.Z. and J.Y. helped to revise the paper. Y.H., L.Y. and Q.Y. contributed equally to this work.

Notes

The authors declare no competing financial interest.

ACKNOWLEDGMENTS

We acknowledge that this work was supported by the National Natural Science Foundation of China (11674354), the Anhui Provincial Natural Science Foundation (2008085J22), the Fundamental Research Funds for the Central Universities of China (Grant PA2020GDSK0086), Austrian-Chinese Cooperative R&D projects (GJHZ2046), and Youth Innovation Promotion Association CAS (Y201841).

REFERENCES

(1) Atamian, H. S.; Creux, N. M.; Brown, E. A.; Garner, A. G.; Blackman, B. K.; Harmer, S. L. Circadian Regulation of Sunflower Heliotropism, Floral Orientation, and Pollinator Visits. *Science* **2016**, *353*, 587−590.

(2) Dawson, C.; Vincent, J. F. V.; Rocca, A.-M. How Pine Cones Open. *Nature* **1997**, *390*, 668.

(3) Gorostiza, E. A.; Colomb, J.; Brembs, B. A Decision Underlies Phototaxis in an Insect. *Open Biol.* **2016**, *6*, 160229.

(4) Mirvakili, S. M.; Hunter, I. W. Artificial Muscles: Mechanisms, Applications, and Challenges. *Adv. Mater.* **2018**, *30*, 1704407.

(5) Xiao, Y.; Jiang, Z.; Tong, X.; Zhao, Y. Biomimetic Locomotion of Electrically Powered "Janus" Soft Robots Using a Liquid Crystal Polymer. *Adv. Mater.* **2019**, *31*, 1903452.

(6) Li, J.; Zhang, R.; Mou, L.; Andrade, M. J.; de Hu, X.; Yu, K.; Sun, J.; Jia, T.; Dou, Y.; Chen, H.; Fang, S.; Qian, D.; Liu, Z. Photothermal Bimorph Actuators with In-Built Cooler for Light Mills, Frequency Switches, and Soft Robots. *Adv. Funct. Mater.* **2019**, *29*, 1808995.

(7) Kim, H.; Lee, H.; Ha, I.; Jung, J.; Won, P.; Cho, H.; Yeo, J.; Hong, S.; Han, S.; Kwon, J.; Cho, K. J.; Ko, S. H. Biomimetic Color Changing Anisotropic Soft Actuators with Integrated Metal Nanowire Percolation Network Transparent Heaters for Soft Robotics. *Adv. Funct. Mater.* **2018**, *28*, 1801847.

(8) Hu, Y.; Liu, J.; Chang, L.; Yang, L.; Xu, A.; Qi, K.; Lu, P.; Wu, G.; Chen, W.; Wu, Y. Electrically and Sunlight-Driven Actuator with Versatile Biomimetic Motions Based on Rolled Carbon Nanotube Bilayer Composite. *Adv. Funct. Mater.* **2017**, *27*, 1704388.

(9) Weng, M.; Zhou, P.; Chen, L.; Zhang, L.; Zhang, W.; Huang, Z.; Liu, C.; Fan, S. Multiresponsive Bidirectional Bending Actuators Fabricated by a Pencil-on-Paper Method. *Adv. Funct. Mater.* **2016**, *26*, 7244−7253.

(10) Wang, X. Q.; Tan, C. F.; Chan, K. H.; Lu, X.; Zhu, L.; Kim, S.; Ho, G. W. In-Built Thermo-Mechanical Cooperative Feedback Mechanism for Self-Propelled Multimodal Locomotion and Electricity Generation. *Nat. Commun.* **2018**, *9*, 3438.

(11) Shin, B.; Ha, J.; Lee, M.; Park, K.; Park, G. H.; Choi, T. H.; Cho, K.-J.; Kim, H.-Y. Hygrobot: A Self-Locomotive Ratcheted Actuator Powered by Environmental Humidity. *Sci. Robot.* **2018**, *3*, No. eaar2629.

(12) Mu, J.; Wang, G.; Yan, H.; Li, H.; Wang, X.; Gao, E.; Hou, C.; Pham, A. T. C.; Wu, L.; Zhang, Q.; Li, Y.; Xu, Z.; Guo, Y.; Reichmanis, E.; Wang, H.; Zhu, M. Molecular-Channel Driven Actuator with Considerations for Multiple Configurations and Color Switching. *Nat. Commun.* **2018**, *9*, 590.

(13) Miriyev, A.; Stack, K.; Lipson, H. Soft Material for Soft Actuators. *Nat. Commun.* **2017**, *8*, 596.

(14) Zeng, H.; Wani, O. M.; Wasylczyk, P.; Kaczmarek, R.; Priimagi, A. Self-Regulating Iris Based on Light-Actuated Liquid Crystal Elastomer. *Adv. Mater.* **2017**, *29*, 1701814.

(15) Wehner, M.; Truby, R. L.; Fitzgerald, D. J.; Mosadegh, B.; Whitesides, G. M.; Lewis, J. A.; Wood, R. J. An Integrated Design and Fabrication Strategy for Entirely Soft, Autonomous Robots. *Nature* **2016**, *536*, 451−455.

(16) Amjadi, M.; Sitti, M. High-Performance Multiresponsive Paper Actuators. *ACS Nano* **2016**, *10*, 10202−10210.

(17) Hu, W.; Lum, G. Z.; Mastrangeli, M.; Sitti, M. Small-Scale Soft-Bodied Robot with Multimodal Locomotion. *Nature* **2018**, *554*, 81−85.

(18) Han, B.; Zhang, Y.; Chen, Q.; Sun, H. Carbon-Based Photothermal Actuators. *Adv. Funct. Mater.* **2018**, *28*, 1802235.

(19) Zhang, X.; Yu, Z.; Wang, C.; Zarrouk, D.; Seo, J.-W. T.; Cheng, J. C.; Buchan, A. D.; Takei, K.; Zhao, Y.; Ager, J. W.; Zhang, J.; Hettick, M.; Hersam, M. C.; Pisano, A. P.; Fearing, R. S.; Javey, A. Photoactuators and Motors Based on Carbon Nanotubes with Selective Chirality Distributions. *Nat. Commun.* **2014**, *5*, 2983.

(20) Gelebart, A. H.; Mulder, D. J.; Varga, M.; Konya, A.; Vantomme, G.; Meijer, E. W. Making Waves in a Photoactive Polymer. *Nature* **2017**, *546*, 632−636.

(21) Kumar, K.; Knie, C.; Bléger, D.; Peletier, M. A.; Friedrich, H.; Hecht, S.; Broer, D. J.; Debije, M. G.; Schenning, A. P. H. J. A Chaotic Self-Oscillating Sunlight-Driven Polymer Actuator. *Nat. Commun.* **2016**, *7*, 11975.

(22) Hu, Y.; Li, Z.; Lan, T.; Chen, W. Photoactuators for Direct Optical-to-Mechanical Energy Conversion: from Nanocomponent Assembly to Macroscopic Deformation. *Adv. Mater.* **2016**, *28*, 10548−10556.

(23) Zeng, H.; Lahikainen, M.; Liu, L.; Ahmed, Z.; Wani, O. M.; Wang, M.; Yang, H.; Priimagi, A. Light-Fuelled Freestyle Self-Oscillators. *Nat. Commun.* **2019**, *10*, 5057.

(24) Yang, L.; Chang, L.; Hu, Y.; Huang, M.; Ji, Q.; Lu, P.; Liu, J.; Chen, W.; Wu, Y. An Autonomous Soft Actuator with Light-Driven Self-Sustained Wavelike Oscillation for Phototactic Self-Locomotion and Power Generation. *Adv. Funct. Mater.* **2020**, *30*, 1908842.

(25) Lahikainen, M.; Zeng, H.; Priimagi, A. Reconfigurable Photoactuator through Synergistic Use of Photochemical and Photothermal Effects. *Nat. Commun.* **2018**, *9*, 4148.

(26) Dong, X.; Xu, J.; Xu, X.; Dai, S.; Zhou, X.; Ma, C.; Cheng, G.; Yuan, N.; Ding, J. Sunlight-Driven Continuous Flapping-Wing Motion. *ACS Appl. Mater. Interfaces* **2020**, *12*, 6460−6470.

(27) Wang, S.; Gao, Y.; Wei, A.; Xiao, P.; Liang, Y.; Lu, W.; Chen, C.; Zhang, C.; Yang, G.; Yao, H.; Chen, T. Asymmetric Elastoplasticity of Stacked Graphene Assembly Actualizes Programmable Untethered Soft Robotics. *Nat. Commun.* **2020**, *11*, 4359.

(28) Hu, Y.; Wu, G.; Lan, T.; Zhao, J.; Liu, Y.; Chen, W. A Graphene-Based Bimorph Structure for Design of High Performance Photoactuators. *Adv. Mater.* **2015**, *27*, 7867−7873.

(29) Chen, L.; Weng, M.; Zhou, P.; Huang, F.; Liu, C.; Fan, S.; Zhang, W. Graphene-Based Actuator with Integrated-Sensing Function. *Adv. Funct. Mater.* **2019**, *29*, 1806057.

(30) Cheng, H.; Zhao, F.; Xue, J.; Shi, G.; Jiang, L.; Qu, L. One Single Graphene Oxide Film for Responsive Actuation. *ACS Nano* **2016**, *10*, 9529−9535.

(31) Han, B.; Zhang, Y.; Zhu, L.; Li, Y.; Ma, Z.; Liu, Y.; Zhang, X.; Gao, X.; Chen, Q.; Qiu, C.; Sun, H. Plasmonic-Assisted Graphene Oxide Artificial Muscles. *Adv. Mater.* **2018**, *31*, 1806386.

(32) Yu, X.; Cheng, H.; Zhang, M.; Zhao, Y.; Qu, L.; Shi, G. Graphene-Based Smart Materials. *Nat. Rev. Mater.* **2017**, *2*, 17046.

(33) Mu, J.; Hou, C.; Wang, H.; Li, Y.; Zhang, Q.; Zhu, M. Origami-Inspired Active Graphene-Based Paper for Programmable Instant Self-Folding Walking Devices. *Sci. Adv.* **2015**, *1*, No. e1500533.

(34) Cheng, Y.; Chan, K. H.; Wang, X.; Ding, T.; Li, T.; Lu, X.; Ho, G. W. Direct-Ink-Write 3D Printing of Hydrogels into Biomimetic Soft Robots. *ACS Nano* **2019**, *13*, 13176−13184.

(35) Wang, X.; Chan, K. H.; Cheng, Y.; Ding, T.; Li, T.; Achavananthadith, S.; Ahmet, S.; Ho, J. S.; Ho, G. W. Somatosensory, Light-Driven, Thin-Film Robots Capable of Integrated Perception and Motility. *Adv. Mater.* **2020**, *32*, 2000351.

(36) Zhang, Q.; Zhang, J. Q.; Wan, S. Y.; Wang, W. Y.; Fu, L. Stimuli-Responsive 2D Materials Beyond Graphene. *Adv. Funct. Mater.* **2018**, *28*, 1802500.

https://dx.doi.org/10.1021/acsnano.0c10797
ACS Nano 2021, 15, 5294−5306

(37) Naguib, M.; Kurtoglu, M.; Presser, V.; Lu, J.; Niu, J.; Heon, M.; Hultman, L.; Gogotsi, Y.; Barsoum, M. W. Two-Dimensional Nanocrystals Produced by Exfoliation of Ti3AlC2. *Adv. Mater.* **2011**, *23*, 4248−4253.
(38) Fan, X.; Ding, Y.; Liu, Y.; Liang, J.; Chen, Y. Plasmonic $Ti_3C_2T_x$ MXene Enables Highly-Efficient Photothermal Conversion for Healable and Transparent Wearable Device. *ACS Nano* **2019**, *13*, 8124−8134.
(39) Naguib, M.; Mashtalir, O.; Carle, J.; Presser, V.; Lu, J.; Hultman, L.; Gogotsi, Y.; Barsoum, M. W. Two-Dimensional Transition Metal Carbides. *ACS Nano* **2012**, *6*, 1322−1331.
(40) Iqbal, A.; Shahzad, F.; Hantanasirisakul, K.; Kim, M.; Kwon, J.; Hong, J.; Kim, H.; Kim, D.; Gogotsi, Y.; Koo, C. M. Anomalous Absorption of Electromagnetic Waves by 2D Transition Metal Carbonitride Ti3CNTx (MXene). *Science* **2020**, *369* (6502), 446−450.
(41) Xu, D.; Li, Z.; Li, L.; Wang, J. Insights into the Photothermal Conversion of 2D MXene Nanomaterials: Synthesis, Mechanism, and Applications. *Adv. Funct. Mater.* **2020**, *30*, 2000712.
(42) Li, R.; Zhang, L.; Shi, L.; Wang, P. MXene Ti_3C_2: An Effective 2D Light-to-Heat Conversion Material. *ACS Nano* **2017**, *11*, 3752−3759.
(43) Ghidiu, M.; Halim, J.; Kota, S.; Bish, D.; Gogotsi, Y.; Barsoum, M. W. Ion-Exchange and Cation Solvation Reactions in Ti_3C_2 MXene. *Chem. Mater.* **2016**, *28*, 3507−3514.
(44) Wang, J.; Liu, Y.; Cheng, Z.; Xie, Z.; Yin, L.; Wang, W.; Song, Y.; Zhang, H.; Wang, Y.; Fan, Z. Highly Conductive MXene Film Actuator Based on Moisture Gradients. *Angew. Chem., Int. Ed.* **2020**, *59*, 14029−14033.
(45) Nguyen, V. H.; Tabassian, R.; Oh, S.; Nam, S.; Mahato, M.; Thangasamy, P.; Rajabi-Abhari, A.; Hwang, W.; Taseer, A. K.; Oh, I.-K. Stimuli-Responsive MXene-Based Actuators. *Adv. Funct. Mater.* **2020**, *30*, 1909504.
(46) Cao, J.; Zhou, Z.; Song, Q.; Chen, K.; Su, G.; Zhou, T.; Zheng, Z.; Lu, C.; Zhang, X. Ultrarobust $Ti_3C_2T_x$ MXene-Based Soft Actuators *via* Bamboo-Inspired Mesoscale Assembly of Hybrid Nanostructures. *ACS Nano* **2020**, *14*, 7055−7065.
(47) Cai, G.; Ciou, J.-H.; Liu, Y.; Jiang, Y.; Lee, P. S. Leaf-Inspired Multiresponsive MXene-Based Actuator for Programmable Smart Devices. *Sci. Adv.* **2019**, *5*, No. eaaw7956.
(48) Umrao, S.; Tabassian, R.; Kim, J.; Nguyen, V. H.; Zhou, Q.; Nam, S.; Oh, I.-K. MXene Artificial Muscles Based on Ionically Cross-Linked $Ti_3C_2T_x$ Electrode for Kinetic Soft Robotics. *Sci. Robot.* **2019**, *4*, No. eaaw7797.
(49) Xie, Y.; Hill, C. A. S.; Xiao, Z.; Militz, H.; Mai, C. Silane Coupling Agents Used for Natural Fiber/Polymer Composites: A Review. *Composites, Part A* **2010**, *41*, 806−819.
(50) Shen, C.; Kong, G.; Wang, J.; Zhang, X. Synthesis and Characterization of High Temperature Proton Exchange Membrane from Isocyanatopropyltriethoxysilane and Hydroxyethane Diphosphonic Acid. *Int. J. Hydrogen Energy* **2015**, *40*, 363−372.
(51) Hamerton, I.; Hay, J. N.; Jones, J. R.; Lu, S. Y. Covalent Incorporation of 2,5-Diphenyloxazole in Sol-Gel Matrices and Their Application in Radioanalytical Chemistry. *Chem. Mater.* **2000**, *12*, 568−572.
(52) Jo, S.; Park, K. Surface Modification Using Silanated Poly(ethylene glycol)s. *Biomaterials* **2000**, *21*, 605−616.
(53) Peng, C.; Li, J.; Li, Z.; Wu, Z.; Zhou, D. Synthesis of SiO_2/Epoxy-Benzoxazine Ternary Copolymer *via* Sol-Gel Method: Thermal and Mechanical Behavior. *Mater. Des.* **2016**, *111*, 453−462.
(54) Yang, Y.; Cao, Z.; He, P.; Shi, L.; Ding, G.; Wang, R.; Sun, J. $Ti_3C_2T_x$ MXene-Graphene Composite Films for Wearable Strain Sensors Featured with High Sensitivity and Large Range of Linear Response. *Nano Energy* **2019**, *66*, 104134.
(55) Di, Z.; Shimai, S.; Zhao, J.; Jin, D.; Zhang, J.; Zhou, G.; Liu, J.; Wang, S. Density Difference in Pressure-Filtrated Wet Cakes Produced from Spontaneous Gelling Slurries. *J. Am. Ceram. Soc.* **2020**, *103*, 1396−1403.
(56) Tiller, F.; Tsai, C. Theory of Filtration of Ceramics: I, Slip Casting. *J. Am. Ceram. Soc.* **1986**, *69*, 882−887.
(57) Muckley, E. S.; Naguib, M.; Wang, H.-W.; Vlcek, L.; Osti, N. C.; Sacci, R. L.; Sang, X.; Unocic, R. R.; Xie, Y.; Tyagi, M.; Mamontov, E.; Page, K. L.; Kent, P. R. C.; Nanda, J.; Ivanov, I. N. Multimodality of Structural, Electrical, and Gravimetric Responses of Intercalated MXenes to Water. *ACS Nano* **2017**, *11*, 11118−11126.
(58) Hu, Y.; Xu, A.; Liu, J.; Yang, L.; Chang, L.; Huang, M.; Gu, W.; Wu, G.; Lu, P.; Chen, W.; Wu, Y. Multifunctional Soft Actuators Based on Anisotropic Paper/Polymer Bilayer Toward Bioinspired Applications. *Adv. Mater. Technol.* **2019**, *4*, 1800674.

https://dx.doi.org/10.1021/acsnano.0c10797
ACS Nano 2021, 15, 5294−5306